J. Appl. Comput. Mech., xx(x) (2026) 1-7
DOI: 10.22055/jacm.2026.48780.5495

ISSN: 2383-4536
jacm.scu.ac.ir

Shahid Chamran University of Ahvaz

Journal of Applied and Computational Mechanics

Research Paper

A Power-Equivalence-Based Computational Method for Homogenized Equivalent Conductivity of Laminated Composites

Siyuan Han[1], Guoqiang Yu[1], Xiguang Gao[1], Chenggang Li[2], Yingdong Song[1,3]

[1] Key Laboratory of Aero-engine Thermal Environment and Structure, Ministry of Industry and Information Technology, College of Energy and Power Engineering, Nanjing University of Aeronautics and Astronautics, Nanjing 210016, P.R. China, Email: hansiyuan@nuaa.edu.cn (S.H.); ygq@nuaa.edu.cn (G.Y.); gaoxiguang@nuaa.edu.cn (X.G.)

[2] Taihang National Laboratory, Chengdu 610504, P.R. China, Email: Lichenggang606@163.com

[3] Harbin Engineering University, Harbin, 150001, P.R. China, Email: ydsong@nuaa.edu.cn

Received September 24 2025; Revised February 22 2026; Accepted for publication March 24 2026.
✉ Corresponding author: G. Yu (ygq@nuaa.edu.cn)

Abstract. Electrical resistivity tomography (ERT) has been widely applied in recent years for damage monitoring in composite materials, particularly in laminated plates. The prevailing approach in ERT-based laminate monitoring simplifies the analysis by treating composites as orthotropic materials, which contain solely 0° and 90° oriented layers. However, this orthotropic assumption becomes invalid for actual composite layups with arbitrary ply orientations. To address this problem, this paper proposes a homogenized equivalent conductivity calculation method for laminated composites based on power equivalence. This method enables solving equivalent conductivity for laminates with arbitrary layup configurations, thereby allowing substitution of the original layered model with a homogenized plate model. Comparative FEM analyses of various laminate configurations confirm that the boundary voltage distributions obtained using the homogenized conductivity model match the actual layered structure results within 1.2% mean absolute error.

Keywords: Structural health monitoring, Laminated composite, Equivalent conductivity, Electrical resistivity tomography.

1. Introduction

Laminated plates, as fundamental structural elements in composite engineering, find broad applications in aerospace, renewable energy, and other advanced engineering fields [1-3]. However, upon impact, laminated structures may develop various damage modes including delamination, matrix cracking, and fiber breakage [4-6], necessitating effective damage monitoring techniques to assess structural integrity. As an emerging non-destructive testing technique, electrical resistivity tomography (ERT) has garnered significant attention in composite damage detection in recent years, owing to its non-invasive nature, rapid response, and simple equipment configuration [7-9].

In ERT systems, multiple electrodes are typically arranged around the target object. A weak current is injected into the object through these electrodes as excitation, while the resulting boundary voltages are simultaneously measured (known as the ERT forward problem). These voltages are then used to reconstruct the spatial distribution of electrical parameters within the target object (known as the ERT inverse problem), with the final reconstructed parameter distribution visualized as a color contour map. The complete working principle of ERT is illustrated in Fig. 1.

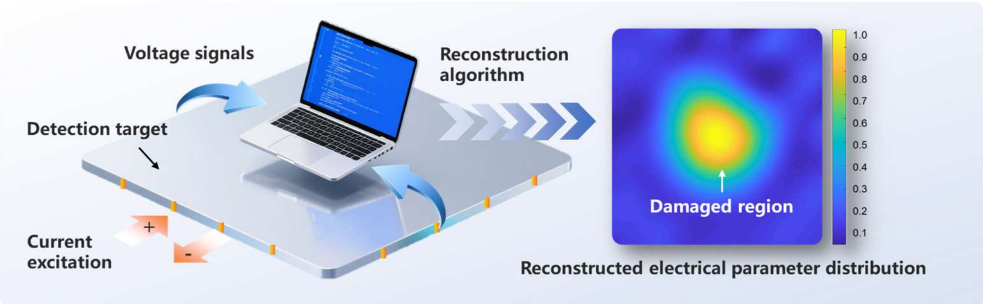

Fig. 1. Complete working principle of ERT.

Published online: March 27 2026

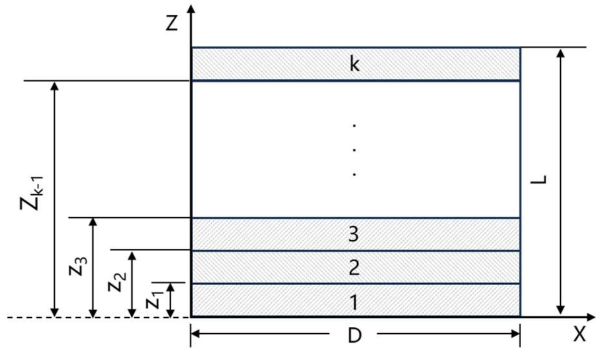

Fig. 2. Diagram of the laminated model.

Accurate computation of the boundary voltage response under current excitation is critical for solving the ERT forward problem. The prevailing approach in ERT-based laminate monitoring simplifies the analysis by treating composites as orthotropic materials, which contain solely 0° and 90° oriented layers. Under this condition, the material's overall conductivity tensor reduces to a diagonal matrix. However， practical engineering structures incorporate diverse ply orientations (e.g., quasi-isotropic [0°/±45°/90°]s stacks), and the conductivity matrix of the laminate may no longer remain a simple diagonal matrix.

Under such conditions, accurate computation of the target's electrical response to excitation can only be achieved through layer-by-layer finite element discretization of the structure, which will significantly increase the computational cost of solving ERT problems. To address this problem, this paper proposes a homogenized equivalent conductivity calculation method for laminated composites based on power equivalence. This method can be applicable to laminates with arbitrary ply orientations and layer thicknesses. The derived equivalent conductivity enables substitution of the multilayer model with a homogeneous representation, leading to significant reduction in FEM mesh density.

2. Computational Framework for Equivalent Electrical Conductivity of Laminated Composites

2.1. Basic assumptions

The laminate model established in this study is illustrated in Fig. 2. Drawing analogy to the classical laminate plate theory in elasticity mechanics [10], the following assumptions are made for the laminate:

1) Perfect interfacial contact is maintained between adjacent plies in the laminate, ensuring continuous electric field distribution across layer boundaries.
2) The stacked laminate remains compliant with the thin-plate assumption (where the thickness-to-span ratio L/D is less than 0.1). Under this assumption, the electric field intensity can be considered constant along the Z direction.
3) The laminate and its equivalent homogeneous substitute achieve electrical equivalence when they dissipate identical Joule heat under the same boundary conditions.

2.2. Formula derivation

The power density $\boldsymbol{P}$ is calculated by Eq. (1) as follows:

$$\boldsymbol{P} = \boldsymbol{E} \cdot \boldsymbol{J} \tag{1}$$

where $\boldsymbol{E}$ denotes the electric field intensity and $\boldsymbol{J}$ represents the current density. The relationship between current density and material conductivity $\boldsymbol{\sigma}$ is given by Eq. (2):

$$\boldsymbol{J} = \boldsymbol{\sigma} \cdot \boldsymbol{E} \tag{2}$$

Hence, Eq. (1) can be further reformulated as follows:

$$\boldsymbol{P} = \boldsymbol{E}^{\boldsymbol{T}} \cdot \boldsymbol{\sigma} \cdot \boldsymbol{E} \tag{3}$$

Assuming the ply material exhibits orthotropic conductivity, the conductivity tensor $\boldsymbol{\sigma_k}$ of the k-th ply layer can be expressed in the following form:

$$\boldsymbol{\sigma_k} = \begin{bmatrix} \sigma_k^{11} & 0 & 0 \\ 0 & \sigma_k^{22} & 0 \\ 0 & 0 & \sigma_k^{33} \end{bmatrix} \tag{4}$$

When the ply orientation angle is θ, the conductivity matrix in the global coordinate system transforms to the following form:

$$\boldsymbol{\sigma_k^\theta} = \boldsymbol{R}(\theta) \cdot \boldsymbol{\sigma_k} \cdot \boldsymbol{R}(\theta)^T \tag{5}$$

where the rotation matrix $\boldsymbol{R}(\theta)$ is given by the following expression:

$$\boldsymbol{R}(\theta) = \begin{bmatrix} cos\theta & -sin\theta & 0 \\ sin\theta & cos\theta & 0 \\ 0 & 0 & 1 \end{bmatrix} \tag{6}$$

Integrating the power density along the thickness direction (Z-direction) yields the thermal power $\boldsymbol{Q_k}$ of the k-th ply layer as follows:

$$\boldsymbol{Q_k} = \int_{z_{k-1}}^{z_k} \boldsymbol{E^T} \boldsymbol{\sigma_k^\theta} \boldsymbol{E} \, dz \tag{7}$$

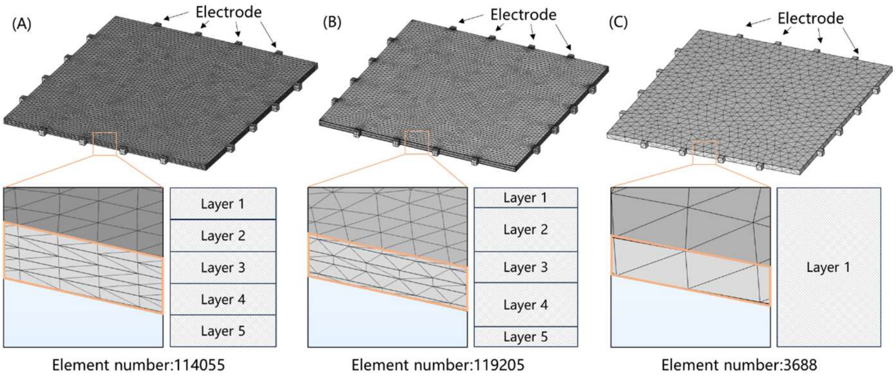

Fig. 3. Three finite element models for electrical response computation.

By analogy with Eq. (7), layer-wise integration through the laminate thickness yields the total thermal power of the stacked laminate as follows:

$$\boldsymbol{Q_{total}} = \int_0^{z_1} \boldsymbol{E}^T \boldsymbol{\sigma}_1^{\theta} \boldsymbol{E}\, dz + \int_{z_1}^{z_2} \boldsymbol{E}^T \boldsymbol{\sigma}_2^{\theta} \boldsymbol{E}\, dz + \cdots + \int_{z_{k-1}}^{z_k} \boldsymbol{E}^T \boldsymbol{\sigma}_k^{\theta} \boldsymbol{E}\, dz \tag{8}$$

Based on assumption (3) in Section 2.1, the thermal power generated by the equivalent homogeneous plate should equal that of the stacked laminate, leading to the following equation:

$$\int_0^{L} \boldsymbol{E}^T \boldsymbol{\sigma_{equal}} \boldsymbol{E}\, dz = \int_0^{z_1} \boldsymbol{E}^T \boldsymbol{\sigma}_1^{\theta} \boldsymbol{E}\, dz + \cdots + \int_{z_{k-1}}^{z_k} \boldsymbol{E}^T \boldsymbol{\sigma}_k^{\theta} \boldsymbol{E}\, dz \tag{9}$$

Equation (9) can be further simplified to Eq. (10):

$$\boldsymbol{\sigma_{equal}} = \left(\int_0^{z_1} \boldsymbol{\sigma}_1^{\theta}\, dz + \cdots + \int_{z_{k-1}}^{z_k} \boldsymbol{\sigma}_k^{\theta}\, dz \right) / L \tag{10}$$

Using Eqs. (5), (6), (10), the equivalent conductivity of the homogenized plate can be calculated given the ply material conductivity, ply orientation angles, and layer thicknesses.

If the actual laminate structure does not satisfy the thin plate assumption and it is necessary to consider the internal electric field distortion caused by interlaminar coupling effects, Eq. (10) needs to be rewritten as follows:

$$\boldsymbol{\sigma_{equal}} = \left(\int_0^{z_1} \boldsymbol{E}_1^T \boldsymbol{\sigma}_1^{\theta} \boldsymbol{E}_1\, dz + \cdots + \int_{z_{k-1}}^{z_k} \boldsymbol{E}_k^T \boldsymbol{\sigma}_k^{\theta} \boldsymbol{E}_k\, dz \right) / (L \cdot \boldsymbol{E}^T \boldsymbol{E}) \tag{11}$$

where $\boldsymbol{E_1}, \ldots, \boldsymbol{E_k}$ are the electric field strengths of each layer.

2.3. Validation

This study designs five laminate models as verification cases, with each case configured with a 5-ply stacking sequence. The test cases encompass various configurations including symmetric/asymmetric stacks, uniform/non-uniform thickness stacks, ensuring methodological generality.

To meet computational requirements, this study develops three finite element models (labeled as A, B, and C) with distinct configurations using simulation software (This paper achieves model establishment and subsequent numerical calculations based on COMSOL Multiphysics 6.0), as illustrated in Fig. 3. Sixteen electrodes were arranged around the model to inject currents and record boundary voltages. The laminate has a side length of 40 mm and a total thickness of 1 mm. The electrodes are 1 mm in both height and width, with a conductivity of 1 S/m, and are uniformly spaced at 8 mm intervals. Specifically, Laminate Models 1-4 correspond to FEM Model A (uniform ply-thickness), Laminate Model 5 aligns with FEM Model B (variable ply-thickness), and the homogenized plate is represented by FEM Model C (single-layer).

The conductivity values of ply materials used in this study are listed below (Unit: S/m):

$$\boldsymbol{\sigma_k} = \begin{bmatrix} 0.1 & 0 & 0 \\ 0 & 1 & 0 \\ 0 & 0 & 1 \end{bmatrix} \tag{12}$$

Application of the Section 2.1 algorithm to Table 1 stack laminate yields the equivalent resistivity matrix in Table 2.

Table 1. Stack information of laminate models.

Model number	Stack information	
1	Ply angle	[0°/45°/90°/45°/0°]
	Ply thickness (mm)	[0.2 /0.2 /0.2 /0.2 /0.2]
2	Ply angle	[45°/-45°/0°/-45°/45°]
	Ply thickness (mm)	[0.2 /0.2 /0.2 /0.2 /0.2]
3	Ply angle	[30°/45°/90°/-45°/-30°]
	Ply thickness (mm)	[0.2 /0.2 /0.2 /0.2 /0.2]
4	Ply angle	[0°/30°/45°/60°/90°]
	Ply thickness (mm)	[0.2 /0.2 /0.2 /0.2 /0.2]
5	Ply angle	[0°/90°/0°/90°/0°]
	Ply thickness (mm)	[0.1 /0.3 /0.2 /0.3 /0.1]

Table 2. Calculated equivalent conductivity of different laminate models.

Model number	Equivalent conductivity (S/m)
1	$\begin{bmatrix} 0.46 & 0 & 0 \\ 0 & 0.64 & 0 \\ 0 & 0 & 1 \end{bmatrix}$
2	$\begin{bmatrix} 0.46 & 0 & 0 \\ 0 & 0.46 & 0 \\ 0 & 0 & 1 \end{bmatrix}$
3	$\begin{bmatrix} 0.55 & 0 & 0 \\ 0 & 0.55 & 0 \\ 0 & 0 & 1 \end{bmatrix}$
4	$\begin{bmatrix} 0.55 & -0.24588 & 0 \\ -0.24588 & 0.55 & 0 \\ 0 & 0 & 1 \end{bmatrix}$
5	$\begin{bmatrix} 0.64 & 0 & 0 \\ 0 & 0.46 & 0 \\ 0 & 0 & 1 \end{bmatrix}$

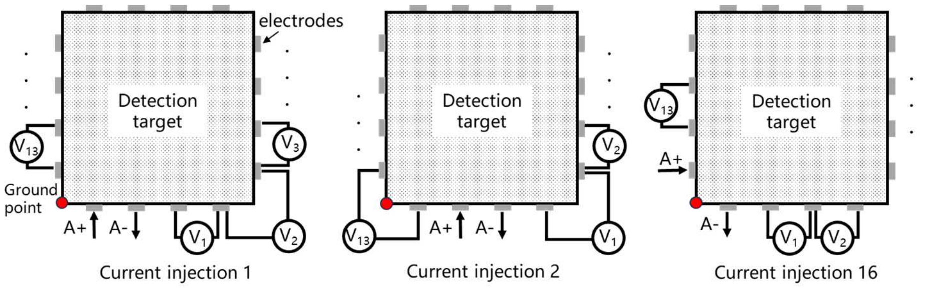

Fig. 4. Adjacent-pattern protocol.

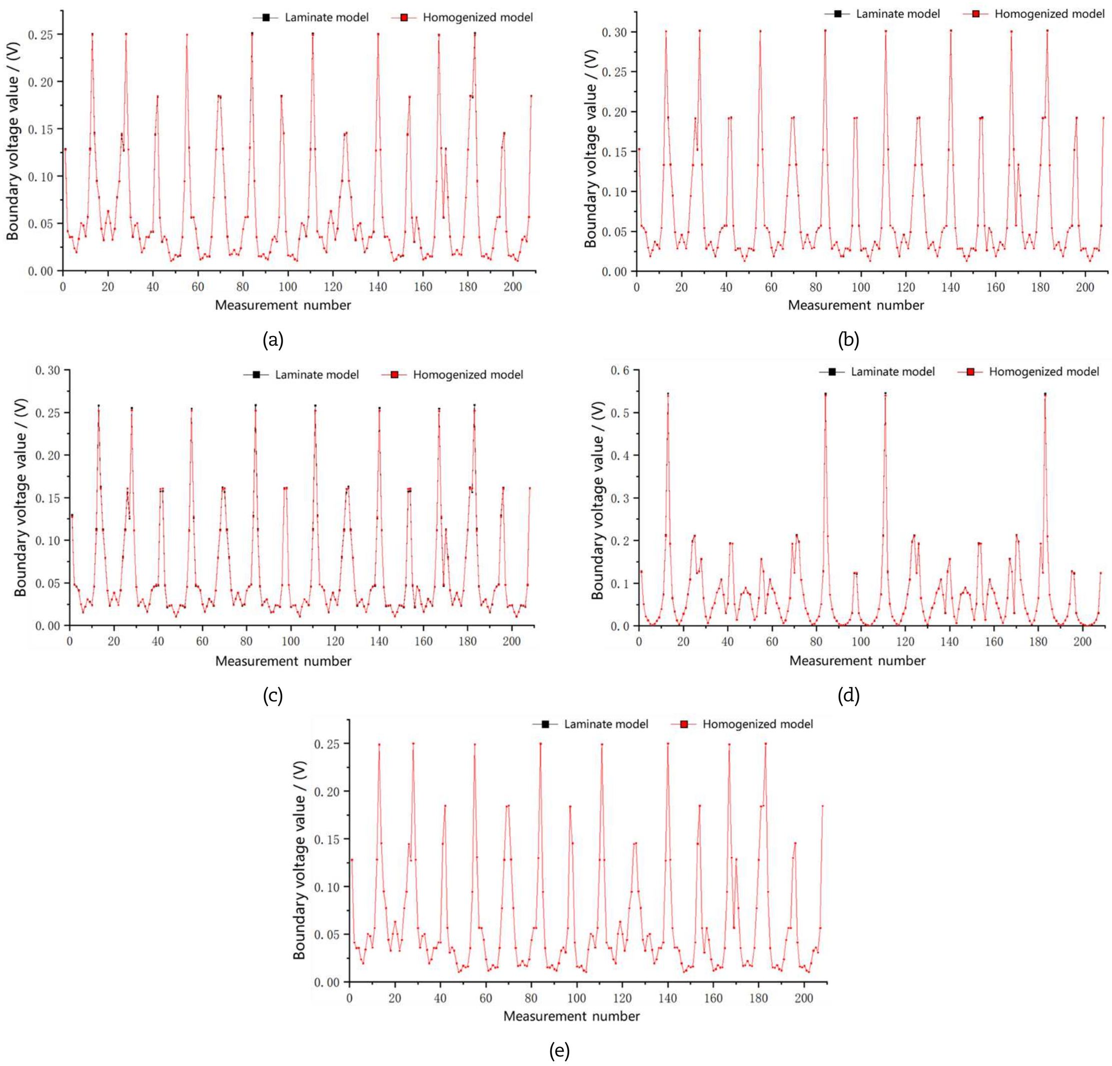

Fig. 5. Comparison of boundary voltage responses between laminate models and their equivalent homogenized models, (a) Model 1, (b) Model 2, (c) Model 3, (d) Model 4, (e) Model 5.

Table 3. Errors in boundary voltage calculations between homogenized models and laminate models.

Model number	Average error e
1	0.3617%
2	0.1116%
3	1.2171%
4	0.8707%
5	0.1216%

This study employs the adjacent pattern to apply current excitation and boundary voltages acquisition for both laminate model and homogenized model. The adjacent-pattern protocol executes 16 distinct current injection, each followed by 13 boundary voltages acquired (see Fig. 4). Following this protocol, a complete excitation sequence yields 208 boundary voltage values (with unified parameters: 1A excitation current and the bottom-left corner set as zero-potential reference). The final computed boundary voltage results are presented in Fig. 5. (Note: Original negative voltage values were uniformly inverted for visualization purposes).

The relative errors of the five boundary voltage data sets are calculated as follows:

$$e = \left(\sum_{i=1}^{208} |U_i - V_i| / U_i \right) / 208 \tag{13}$$

where the subscript i denotes the i-th voltage data point, vector U represents the simulated boundary voltage results of the laminate model, and vector V corresponds to the homogenized model. The calculated errors are presented in Table 3:

As observed from Fig. 5 (a)-(e) and Table 3, the boundary voltages calculated using the homogenized models show excellent agreement with those from the laminate models, with a maximum error of 1.2171%. Moreover, partial errors originate from numerical deviations caused by differences in finite element mesh density between the homogenized models and the laminate models. In summary, these results validate both the correctness of the proposed equivalent conductivity method and the rationality of the foundational assumptions made in Section 2.1.

3. Application Case: ERT-based Internal Defect Localization in Laminate

3.1. ERT algorithm formula

This paper selected the Newton's One-Step Error Reconstructor (NOSER) [11] as the ERT reconstruction algorithm, and its computational formula is shown below:

$$\Delta\boldsymbol{\rho} = -\left(\boldsymbol{S}^T\boldsymbol{S} + \alpha diag(\boldsymbol{S}^T\boldsymbol{S})\right)^{-1} \cdot \boldsymbol{S}^T \cdot (\boldsymbol{V_{defect}} - \boldsymbol{V_{origen}}) \tag{14}$$

where $\Delta\boldsymbol{\rho}$ is the vector of the nominal resistivity change rate, reflecting the amplitude of the resistivity variation at different macroscopic locations within the laminate, α is the regularization parameter (Based on reference [12], α is uniformly set to 0.1 in this study), $\boldsymbol{V_{defect}}$ and $\boldsymbol{V_{origen}}$ represent the boundary voltages of the laminate with and without defects, respectively. $\boldsymbol{S}$ denotes the sensitivity matrix, which can be solved using the adjoint field method [13]:

$$\boldsymbol{S} = \frac{\partial V_{ij}}{\partial \rho_e} = -\int_{\Omega_e} (\nabla\varphi^i \cdot \nabla\varphi^j) \cdot {\rho_e}^{-1} \, dV \tag{15}$$

where V_{ij} represents the voltage measurement from the j-th measurement under the i-th current injection. Ω_e is the spatial domain of the e-th element. $\nabla\varphi^i$ denotes the electric potential gradient of the element in the excitation field, and $\nabla\varphi^j$ corresponds to the electric potential gradient of the element in the adjoint field. ρ_e is the nominal resistivity of the e-th element and is a scalar quantity.

3.2. Laminate model with internal defect

This paper introduced a localized porosity defect into Model 1 (as shown in Table 1) to serve as the detection target for ERT. As shown in Fig. 6, the defect was introduced between the 2nd and 3rd plies, and the electrical conductivity parameters of each ply are consistent with those defined in Eq. (12). Consistent with Section 2.3, the adjacent stimulation pattern was used to acquire the boundary voltages of the laminate, which were then substituted as $\boldsymbol{V_{defect}}$ into Eq. (14).

3.3. ERT image reconstruction

Boundary voltages of the intact Model 1 were calculated using the laminate model and the homogenized model, respectively. The resulting voltage values were recorded as $\boldsymbol{V_{origen\_1}}$ and $\boldsymbol{V_{origen\_2}}$, and then substituted into Eq. (14) to compute the resistivity distribution. The final ERT image reconstruction results are shown in Fig. 7.

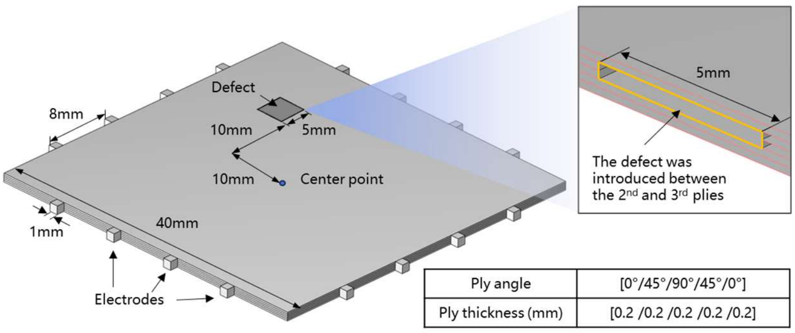

Fig. 6. Laminate model with internal defect.

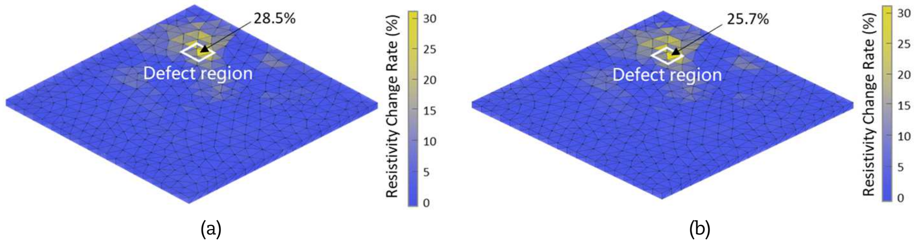

Fig. 7. ERT image reconstruction results: (a) Image reconstructed from voltage of laminate model, (b) Image reconstructed from voltage of homogenized model.

To eliminate the influence of specific material properties on the final results, this paper uses the resistivity change rate to quantify the impact of introduced delamination defects on the resistivity at different locations of the tested object on a macroscopic scale. Here, 0 indicates that the macroscopic resistivity of the material remains unaffected. As can be seen from Fig. 7, the introduction of delamination defects leads to an increase in local resistivity of the material at a macroscopic scale. The elements corresponding to the maximum resistivity change rate in both ERT images are located within the actual defect region. The maximum resistivity change rate in the defect region reconstructed using the boundary voltage from the laminate model is 28.5%, while that reconstructed based on the boundary voltage from the homogenized model is 25.7%, resulting in a computational error of 9.8%. Due to the severely ill-posed nature of the ERT problem [14-16], where minor changes in boundary voltages can cause significant alterations in the final resistivity reconstruction results, this computational error is considered acceptable. In future work, if the mapping relationship between the damage degree of laminate materials and the resistivity change rate can be further established, the calculation method proposed in this paper, combined with ERT technology, can be utilized to achieve rapid structural health monitoring of laminate structures.

4. Conclusion

To improve the monitoring efficiency of ERT for laminate structures, this study proposed a power-equivalence-based homogenization method to compute the equivalent conductivity of multidirectional laminates. The main conclusions are as follows:

1) The boundary voltages calculated using the homogenized models show excellent agreement with those from the laminate models, with a maximum mean error of 1.2171% across five test cases. Meanwhile, the homogenized model requires only 3% of the elements needed for the original laminate model.
2) The assumption that the electric field intensity remains approximately uniform across the thickness of thin-plate structures is validated as reasonable. When it comes to thick-plate targets, where internal electric field distortion due to interlaminar coupling effects needs to be considered, the algorithm must be modified based on the actual electric field intensity distribution.
3) The equivalent conductivity calculation method proposed in this study eliminates the need for layer-by-layer finite element discretization when calculating the electrical response of laminates, thereby significantly reducing the required mesh density and computational cost for solving ERT problems.

Author Contributions

S. Han wrote original draft, developed the mathematical modeling, planned the scheme. G. Yu examined the theory validation, funding acquisition. C. Li was responsible for funding acquisition and investigation. X. Gao initiated the project and contributed to the funding acquisition. Y. Song was responsible for funding acquisition. The manuscript was written through the contribution of all authors. All authors discussed the results, reviewed, and approved the final version of the manuscript.

Acknowledgments

Thanks to Professor Shuguang Li from the University of Nottingham for providing theoretical guidance for this paper.

Conflict of Interest

The authors declared no potential conflicts of interest concerning the research, authorship, and publication of this article.

Funding

This work was supported by the National Natural Science Foundation of China (12572091); National Natural Science Foundation of China (52475158); Postgraduate Research & Practice Innovation Program of Jiangsu Province (KYCX25_0567); China Postdoctoral Science Foundation(2024T171160); Fundamental Research Funds for the Central Universities (NS2024010); Young Elite Scientists Sponsorship Program by CAST (2022QNRC001).

Data Availability Statements

The datasets generated and/or analyzed during the current study are available from the corresponding author on reasonable request.

Nomenclature

D	Length of laminate [m]	E	Electric intensity [V/m]
L	Total thickness of laminate [m]	P	Power density (W/m^3)
U	Boundary voltage (laminate model) [V]	J	Current density (A/m^2)
V	Boundary voltage (homogenized model) [V]	θ	Ply orientation angle (°)

Z_k	The thickness of the k-th layer [m]	e	Relative error
σ	Conductivity [S/m]	ρ	resistivity [Ω.m]

References

[1] Blecherman, S.S., Stankunas, T.N., Composite Fan Exit Guide Vanes for High Bypass Ratio Gas Turbine Engines, *Journal of Aircraft*, 19(12), 1982, 1032-1034.
[2] Etri, H.E., Korkmaz, M.E., Gupta, M.K., Gunay, M., Xu, J., A state-of-the-art review on mechanical characteristics of different fiber metal laminates for aerospace and structural applications, *International Journal of Advanced Manufacturing Technology*, 123, 2022, 2965-2991.
[3] Bui, V.P., Thitsartarn, W., Liu, E.X., Chuan, J.Y.C., Chua, E.K., EM Performance of Conductive Composite Laminate Made of Nanostructured Materials for Aerospace Application, *IEEE Transactions on Electromagnetic Compatibility*, 57(5), 2015, 1-10.
[4] Hebsur, M.G., Noebe, R.D., Revilock, D.M., Impact Resistance of Lightweight Hybrid Structures for Gas Turbine Engine Fan Containment Application, *Journal of Materials Engineering and Performance*, 12, 2003, 470-479.
[5] Li, X., He, X., Liang, J., Song, Y., Zhang, L., Wang, B., Ma, J., Kong, G., Research Status of 3D Braiding Technology, *Applied Composite Materials*, 29, 2022, 147-157.
[6] Liu, L.L., Xuan, H.J., Chen, G.T., Ye, D., Hong, W.R., Xing, J., Wang, J., Ballistic impact testing and analysis of triaxial braided composite fan case material, *Advanced Materials Research*, 535, 2012, 121-132.
[7] Tallman, T.N., Homa, L., Flores, M., Wertz, J., Damage mapping via electrical impedance tomography in complex AM shapes using mixed smoothness and Bayesian regularization, *Computer Methods in Applied Mechanics and Engineering*, 414, 2023, 116185.
[8] Thomas, A.J., Kim, J.J., Tallman, T.N., Bakis, C.E., Damage detection in self-sensing composite tubes via electrical impedance tomography, *Composites Part B: Engineering*, 177, 2019, 107276.
[9] Gao, X., Wei, T., Dong, H., Song, Y., Damage detection in 2.5 DC/SiC composites using electrical resistance tomography, *Journal of the European Ceramic Society*, 39(13), 2019, 3583-3593.
[10] Gibson, R.F., *Principles of Composite Material Mechanics*, CRC Press, 2016.
[11] Cheney, M., Isaacson, D., Newell, J.C., Simske, S., Goble, J., NOSER: An algorithm for solving the inverse conductivity problem, *International Journal of Imaging Systems and Technology*, 2(2), 1990, 66-75.
[12] Wang, Q., Wang, H., Zhang, R., Wang, J., Zheng, Y., Cui, Z., Yang, C., Image reconstruction based on L1 regularization and projection methods for electrical impedance tomography, *Review of Scientific Instruments*, 83(10), 2012, 104707.
[13] Vauhkonen, P.J., Vauhkonen, M., Savolainen, T., Kaipio, J.P., Three-dimensional electrical impedance tomography based on the complete electrode model, *IEEE Transactions on Biomedical Engineering*, 46(9), 2002, 1150-1160.
[14] Yang, X., Zhang, Y., Chen, H., Ma, G., Wang, X., A Two-Stage Imaging Framework Combining CNN and Physics-Informed Neural Networks for Full-Inverse Tomography: A Case Study in Electrical Impedance Tomography (EIT), *IEEE Signal Processing Letters*, 32, 2025, 1096-1100.
[15] Boo, C.J., Kim, H.C., Kang, M.J., Lee, K.Y., Stochastic optimization approaches to image reconstruction in electrical impedance tomography, *International Conference on Computational Science and Its Applications*, Berlin, Heidelberg: Springer Berlin Heidelberg, 2010.
[16] Goncalves, S., De Munck, J.C., Heethaar, R.M., Lopes da Silva, F.H., Van Dijk, B.W., The application of electrical impedance tomography to reduce systematic errors in the EEG inverse problem-a simulation study, *Physiological Measurement*, 21(3), 2000, 379-393.

ORCID iD

Siyuan Han https://orcid.org/0000-0002-9045-9071
Guoqiang Yu https://orcid.org/0000-0003-4849-839X
Xiguang Gao https://orcid.org/0000-0003-3939-5057

How to cite this article: Han S., et al., A Power-Equivalence-Based Computational Method for Homogenized Equivalent Conductivity of Laminated Composites, *J. Appl. Comput. Mech.*, xx(x), 2026, 1–7. https://doi.org/10.22055/jacm.2026.48780.5495